Epitaxy of (GaN)_{1−x}(ZnO)_{x} Solid-Solution Thin Films with Widely Tunable Chemical Composition and Strong Visible Absorption

Chang Yang, Yasushi Hirose, Takuto Wakasugi, Naoki Kashiwa, Hiroki Kawai, Koichi Yamashita, and Tetsuya Hasegawa

Phys. Rev. Applied **10**, 044001 — Published 1 October 2018

DOI: 10.1103/PhysRevApplied.10.044001

Epitaxy of $(GaN)_{1-x}(ZnO)_x$ Solid Solution Thin Films with Wide Chemical Composition Tunability and Strong Visible Absorption

Chang Yang[1,2,3,*], Yasushi Hirose[1,2,*], Takuto Wakasugi[1], Naoki Kashiwa[1], Hiroki Kawai[4,5], Koichi Yamashita[4], and Tetsuya Hasegawa[1,2]

[1] *Department of Chemistry, The University of Tokyo, Bunkyo-ku, Tokyo 113-0033, Japan*

[2] *Kanagawa Academy of Science and Technology (KAST), Kawasaki 213-0012, Japan*

[3] *Felix-Bloch-Institut für Festkörperphysik, Universität Leipzig, Linnéstr. 5, 04103 Leipzig, Germany*

[4] *Department of Chemical System Engineering, The University of Tokyo, Bunkyo-ku, Tokyo 113-0033 Japan*

[5] *Institute of Memory Technology Research & Development, Toshiba Memory Corporation, 1-1, Shibaura 1-chome, Minato-ku, Tokyo, 105-8001, Japan*

*Corresponding author: yangchangyc@gmail.com; hirose@chem.s.u-tokyo.ac.jp

ABSTRACT

The alloying of wide-bandgap ZnO and GaN causes bandgap reduction, enabling visible-light-driven photocatalysis for high-efficiency water splitting. However, challenges in single-crystal $(GaN)_{1-x}(ZnO)_x$ solid solution synthesis prevent a better understanding of the optical properties and electronic structures. Here, low-temperature epitaxial growth of $(GaN)_{1-x}(ZnO)_x$ thin films with a wide tunability of chemical composition is demonstrated by using a multi-target pulsed laser deposition (PLD) system. The phase pure $(GaN)_{1-x}(ZnO)_x$ solid solution was obtained by alternately depositing GaN and ZnO with the thickness of each GaN/ZnO pair set within one or two unit cells. The bandgap of the solid solution thin films as a function of systematically controlled chemical composition shows asymmetric bowing with a minimum at ~2.0 eV for x=0.65. Furthermore, a large absorption coefficient ($>10^4$ cm^{-1}) in the visible light

region has been observed. The shape of the absorption edge is not consistent with that of a direct-transition semiconductor. First-principles calculation suggested that this inconsistency originates from localization of the valence band maximum on N atoms bonded with Zn. A technique for fabricating high-quality epitaxial $(GaN)_{1-x}(ZnO)_x$ solid solutions is essential for acquiring a deep understanding of the fundamental properties of this system.

I. INTRODUCTION

Photocatalytic solar water splitting using semiconductors is a promising way to generate clean and sustainable hydrogen energy.[1,2] However, the solar to hydrogen conversion efficiency is too low to be practical. To improve the efficiency, the development of a semiconductor photocatalyst with a high visible-light activity is crucial. In 2005, Maeda *et al.* achieved visible-light-driven photocatalytic water splitting with a $(GaN)_{1-x}(ZnO)_x$ solid solution.[3,4] Because the hydrogen conversion efficiency of $(GaN)_{1-x}(ZnO)_x$ under visible light was much higher than those of conventional oxide photocatalysts,[3-6] the discovery has triggered studies of these (oxy)nitrides.[7-10]

An intriguing feature of $(GaN)_{1-x}(ZnO)_x$ is that alloying of the wide-bandgap ZnO and GaN reduces the bandgap.[3-6,10-17] For $(GaN)_{1-x}(ZnO)_x$ nanocrystals with a wide compositional range, the absorption onset energy can be reduced to 2.2 eV for a ZnO-rich composition.[15,18] The mechanism of this bandgap narrowing is, however, still under debate. Possible causes include N 2*p* and Zn 3*d* repulsion,[8,19,20] localized Zn acceptor levels,[21,22] short range local order,[7] or repulsion of conduction bands edges of GaN and ZnO phases[23].

This controversy stems from the fact that the fundamental optical properties of $(GaN)_{1-x}(ZnO)_x$ have not been fully established experimentally. For example, there is a large distribution of the estimated absorption onset energy (See Supplemental Material [24], Fig. S1). Furthermore, the absorption coefficient, which is one of the most essential parameters of a photocatalytic material, was reported only for colloidal solutions of nanocrystals with a specific composition of $(GaN)_{0.27}(ZnO)_{0.73}$.[25] These problems are the result of the synthetic process. $(GaN)_{1-x}(ZnO)_x$ are usually synthesized in a fine powder or nanocrystalline form *via* ammonolysis or combustion.[3-6,10-17,26-31] Hence, their optical properties have been evaluated by diffuse reflectance spectroscopy (DRS). Although DRS is a well-established technique to investigate optical properties of a powder sample, it has the following limitations: 1) The spectral shape is hindered by differences in the scattering factor between the sample and a standard;[32] and 2) the absorption spectrum calculated from DRS does not yield absolute absorption coefficients. Therefore, deeper investigations into the bandgap narrowing of $(GaN)_{1-x}(ZnO)_x$ will require bulk single crystals or thin films to enable conventional optical transmittance and/or reflectance measurements.

Despite extensive studies of $(GaN)_{1-x}(ZnO)_x$, a thin-film synthesis has been scarcely reported.[33,34] Furthermore, the chemical compositions were not evaluated in previous studies where polycrystalline thin films were fabricated by reactive RF magnetron sputtering. Here, we demonstrated epitaxial growth of $(GaN)_{1-x}(ZnO)_x$ solid solutions with a wide range of chemical compositions by using pulsed laser deposition (PLD). The solid solution films exhibited strong visible light absorption, with coefficients on the order of 10^4 cm^{-1}. Spectral shapes of the absorption edges exhibited poor agreement with the Tauc plots that assume a direct transition, which has been used in previous studies. Theoretical calculation suggested that this is due to flat valence-band top caused by the orbital localization on N atoms bonded with Zn. The energy of the absorption edge E_g depended on the chemical composition x, where the lowest E_g~2.0 eV was obtained at x=0.65.

II. EXPERIMENTAL

$(GaN)_{1-x}(ZnO)_x$ thin films were fabricated on atomically flat (0001) planes of α-Al_2O_3 and ZnO substrates by alternately depositing ZnO and GaN with multi-target PLD. Ceramic ZnO pellet and liquid Ga targets were ablated for deposition of ZnO and GaN, respectively. Fig. 1(a) shows the timing chart for the multi-target PLD. Each ZnO or GaN target was synchronized with a 248-nm, 2-Hz KrF excimer laser, a variable laser attenuator (0.5 J-cm^{-2}pulse^{-1} for ZnO, and 2.0 J-cm^{-2}pulse^{-1} for GaN), a piezoelectric leak valve controlling oxygen partial pressure (Oxford Applied Research, PLV-1000; $P_{O2}=1.0\times10^{-4}$ Torr for ZnO, and less than 1.0×10^{-8} Torr for GaN), and an electron cyclotron resonance (ECR) plasma source activating nitrogen gas (Tectra, Gen2; turned on only for GaN). The partial nitrogen pressure P_{N2} during the growth and the input current of the ECR source were 1.0×10^{-4} Torr and 40 mA, respectively.

Thicknesses of the films were determined with a stylus profiler (Veeco, Dektak 6M). Chemical compositions of the thin films were evaluated by energy dispersive X-ray spectroscopy (EDX) on a scanning electron microscope (JEOL, JSM-7100F with JED-2300). The background signal from the substrate was excluded by setting the electron accelerating voltage to 2.5 kV. The probing depth was ~80 nm, as estimated by Monte Carlo simulations.[35] Crystallographic structures of the thin films were characterized by X-ray diffraction (XRD) using a four-axis diffractometer with an area detector (Bruker, D8 Discover with GADDS). The out-of-plane lattice constants were calculated from 0002 diffraction of a wurtzite structure. The in-plane lattice constants were calculated from 10-11 diffraction and the out-of-plane lattice constants calculated above. For 10-11 diffraction measurements, the χ (tilt) and φ (in-plane) angles of the sample were adjusted to detect the diffraction spot on the area detector. Surface morphology of the films were evaluated using an atomic force microscope (AFM) (SII Nanotechnology, SPA400 with SPI4000). Optical transmittance T and reflectance R of the films were measured at room temperature with an ultraviolet–visible spectrometer (JASCO V-670), and optical absorbance A was calculated from $A=(1-R-T)/(1-R)$. The measurements were performed under regular transmittance/reflectance configuration without integration sphere, because the films were so flat that light scattering was negligible. The absorption coefficient α was evaluated from $1-A=\exp(-\alpha\, t)$.

The density functional theory-based first-principles calculation were carried out for $(GaN)_{1-x}(ZnO)_x$ (x=0, 0.25, 0.75, and 1) using the Vienna ab initio simulation package (VASP).[36] For the structural optimization, the projector augmented wave (PAW) method[37] with the local density approximation (LDA) functional[38] was used with a cutoff energy of 500 eV. We also calculated the electronic structure with the LDA+U method, where U for d orbitals of Ga and Zn were set at 8.5 and 8.0 eV, respectively.

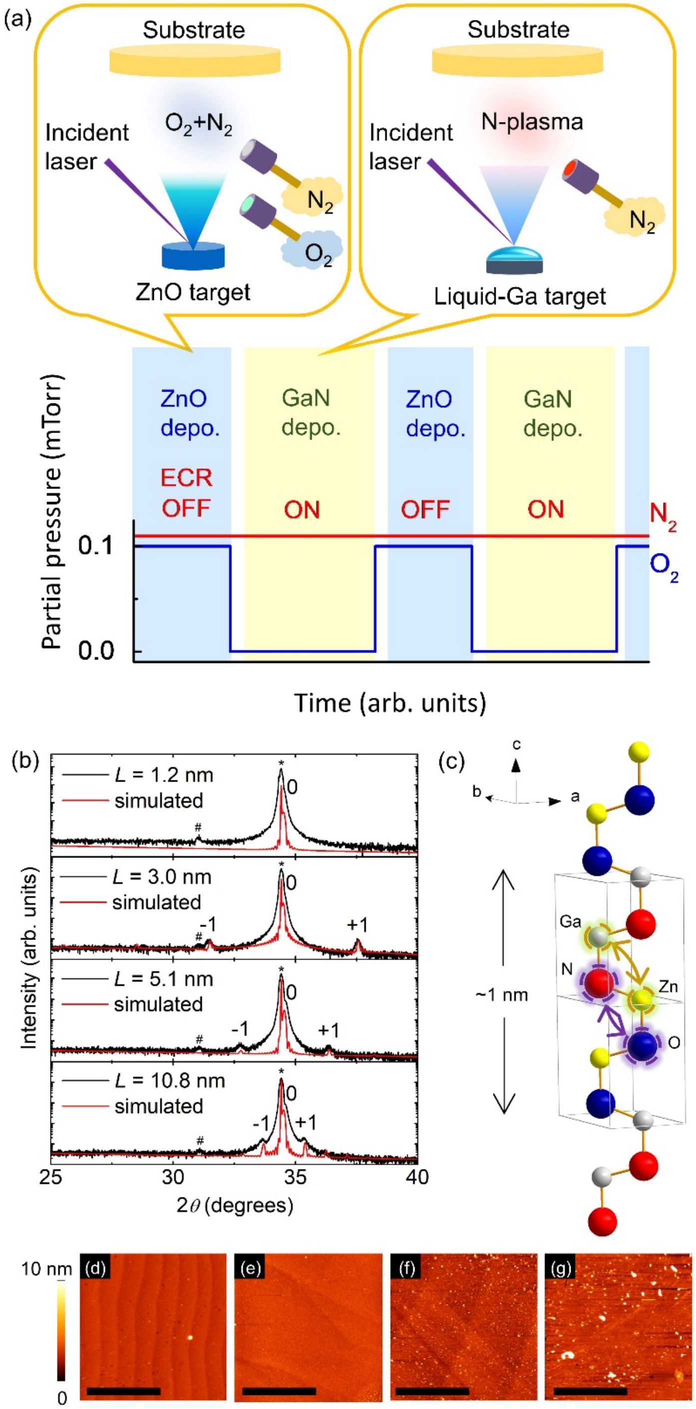

FIG. 1. (a)Schematic of the multi-target PLD system and a timing chart for periodic growth of GaN/ZnO thin films. (b) XRD θ-2θ patterns of GaN/ZnO multilayers grown on ZnO(0001) substrates with different GaN/ZnO pair thicknesses (L). The substrate peaks are marked as asterisk, and the signals from the sample holder are marked as hash sign. The superlattice main peak is denoted by 0, and the first-order satellite peaks are denoted by -1 and +1. (c) Schematic atomic configurations of 1×1×2 wurtzite unit cell of the GaN-ZnO solid solution with possible atom mixing at the cell interfaces. (d-g) AFM images of GaN/ZnO thin films grown on ZnO(0001) substrates with (d) L=1.2 nm, (e) 3.0 nm, (f) 5.1 nm, and (g) 10.8 nm, respectively. Scale bars represent 5 µm.

III. RESULTS AND DISCUSSION

A. Formation of epitaxial solid solutions from superlattices

$(GaN)_{1-x}(ZnO)_x$ thin films were epitaxially grown on (0001) planes of α-Al_2O_3 and ZnO substrates with a multi-target PLD system that alternately deposited ZnO and GaN. The target exchange and gas supply switching were synchronized with a pulsed KrF excimer laser, as illustrated in Fig. 1(a). The total film thickness is ~90 nm. Zn evaporation was suppressed at low growth temperatures, as reported for the bulk synthesis,[31] by keeping the substrates below 100 °C. The $(GaN)_{1-x}(ZnO)_x$ compositions (x) were controlled by the thickness ratio of the sub-layer (ZnO or GaN), allowing a wide chemical composition tunability (x=0.1, 0.3, 0.5, 0.7, and 0.9). For example, the $(GaN)_{0.5}(ZnO)_{0.5}$ film is composed of GaN/ZnO pairs with the thickness ratio of 1:1 for the GaN and ZnO layers in each pair.

We firstly checked influence of the thickness of a GaN/ZnO pair on crystal structure of the obtained films. Fig. 1(b) shows the θ-2θ XRD patterns of the $(GaN)_{0.5}(ZnO)_{0.5}$ samples with different thicknesses of a GaN/ZnO pair from 1 to 10 nm. Owning to the good lattice matching to the substrates, all samples show the (0001) oriented epitaxial growth on ZnO(0001) substrates. When the thickness of a GaN/ZnO pair ranges from 3 to 10 nm, satellite peaks from GaN/ZnO superlattices appeared. The thicknesses of the GaN/ZnO pair calculated from the positions of satellite peaks are consistent well with the designed values (See Supplemental Material [24], Table S1). In contrast, satellite peaks disappeared by reducing the thickness of a GaN/ZnO pair to 1.2 nm, indicating the formation of a solid solution (pseudo-alloy). Considering the fact that the 1.2 nm-thick GaN/ZnO pair includes only 4 layers of GaN and ZnO as illustrated in Fig. 1(c), solid solution was formed probably by interlayer mixing due to relatively high kinetic energy of ablated atoms. AFM observations [Fig. 1(d-g)] revealed that the surfaces of the solid solution films were very smooth, indicating that the formation of the solid solution proceeded homogeneously. Based on these results, we hereafter fixed the thickness of a GaN/ZnO pair at ~1 nm to obtain the solid solution samples.

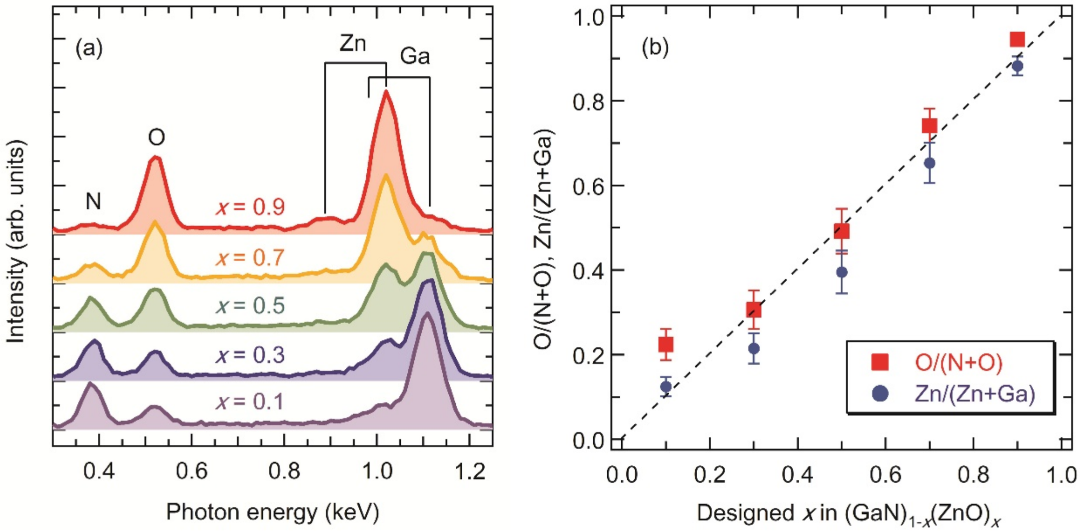

FIG. 2. (a) EDX spectra of $(GaN)_{1-x}(ZnO)_x$ thin films grown on Al_2O_3 substrates. (b) O/(N+O) and Zn/(Zn+Ga) ratios in the $(GaN)_{1-x}(ZnO)_x$ thin films calculated from the EDX spectra plotted against the designed x.

Subsequently, the compositional and structural properties of the $(GaN)_{1-x}(ZnO)_x$ solid solutions were investigated. Fig. 2(a) plots EDX spectra of the $(GaN)_{1-x}(ZnO)_x$ thin films grown on Al_2O_3 substrates. In Fig. 2(b), the O/(N+O) and Zn/(Zn+Ga) ratios in the films, calculated from the spectra, are plotted *vs*. x. The chemical compositions of the films almost agreed with the designed values. The most Ga-rich film (x=0.1) was relatively over-oxidized [O/(N+O)=~0.2], which possibly occurred from oxidation during the period of O_2 supply before the ZnO deposition. The small deviation of the Zn/(Zn+Ga) ratio from the designed value is attributable to a variation of the deposition rate, which might originate from a change of the surface state of the target due to laser ablation. In the following sections, the chemical composition of Zn/(Zn+Ga) was used to distinguish samples.

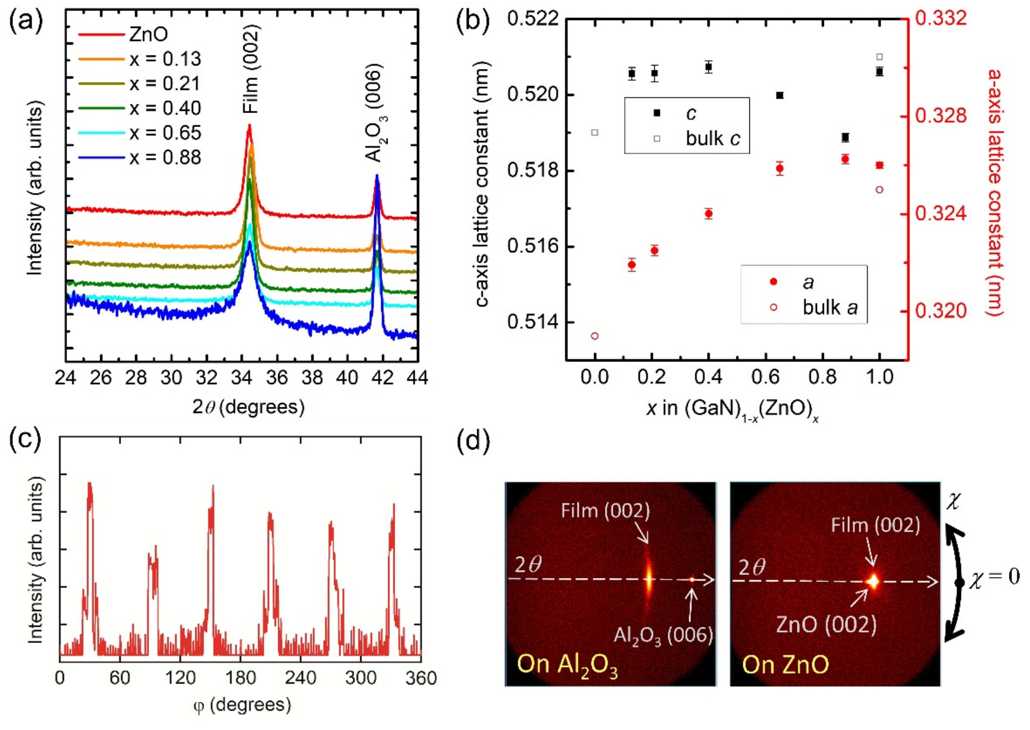

FIG. 3. (a) XRD θ-2θ patterns of $(GaN)_{1-x}(ZnO)_x$ thin films grown on Al_2O_3 substrates. (b) In-plane (a) and out-of-plane (c) lattice constants of $(GaN)_{1-x}(ZnO)_x$ thin films grown on Al_2O_3 substrates against x. (c) A φ scan plot of 10-11 diffraction in XRD patterns of $(GaN)_{1-x}(ZnO)_x$ thin film grown on an Al_2O_3 substrate (x=0.65). (d) Typical XRD two-dimensional detector images of the $(GaN)_{1-x}(ZnO)_x$ thin films on Al_2O_3 and ZnO substrates (x=0.65).

Fig. 3(a) shows XRD patterns of the films grown on Al_2O_3 (0001) substrates. Only 000*l* diffraction peaks from a wurtzite structure were observed without impurities, such as $ZnGa_2O_4$ or Ga_2O_3, or satellite peaks from superlattices. In previous $(GaN)_{1-x}(ZnO)_x$ solid solutions, the lattice parameters monotonically increased with x.[13] Fig. 3(b) plots in-plane and out-of-plane lattice constants of these films. Both lattice constants depended on x, which was generally consistent with previous data.[13] This composition dependent change of lattice constants as well as absence of the satellite peaks indicates that the $(GaN)_{1-x}(ZnO)_x$ films were solid solutions, not a composite or a superlattice of ZnO and GaN. φ-scan plots of 10-11 peaks confirmed clear six-fold symmetry (Fig. 3(c)), indicating epitaxial growth below 100 °C, which was attributable to the high kinetic energy of laser-ablated species (over several eV) and enhanced ZnO and GaN surface migration[39,40] on atomically flat substrates. The crystallinity of the $(GaN)_{1-x}(ZnO)_x$ thin films was improved on the ZnO substrate with better lattice matching, which was confirmed by the reduced peak width along the χ direction of the area detector (Fig. 3(d)).

B. Optical properties of solid solution films

Fig. 4(a) and 4(b) respectively show a photograph and UV-visible absorption spectra of $(GaN)_{1-x}(ZnO)_x$ films grown on Al_2O_3 substrates. All of the films exhibit absorption edges around 2–2.5 eV. The absorption coefficients (α values) were on the order of 10^4 cm^{-1} (Fig. 4(c)), which agrees well with that previously reported for $(GaN)_{0.27}(ZnO)_{0.73}$ nanocrystals (4.6×10^4 cm^{-1} at 2.76 eV).[25] Absorption spectra were also acquired for $(GaN)_{1-x}(ZnO)_x$ thin films grown on ZnO substrates. Those spectra almost coincide with those obtained from films on Al_2O_3 substrates (See Supplemental Material [24], Fig. S2). However, the ZnO substrate exhibited strong absorption in the UV (>3 eV); thus, only absorption spectra of films grown on Al_2O_3 substrates will be considered below.

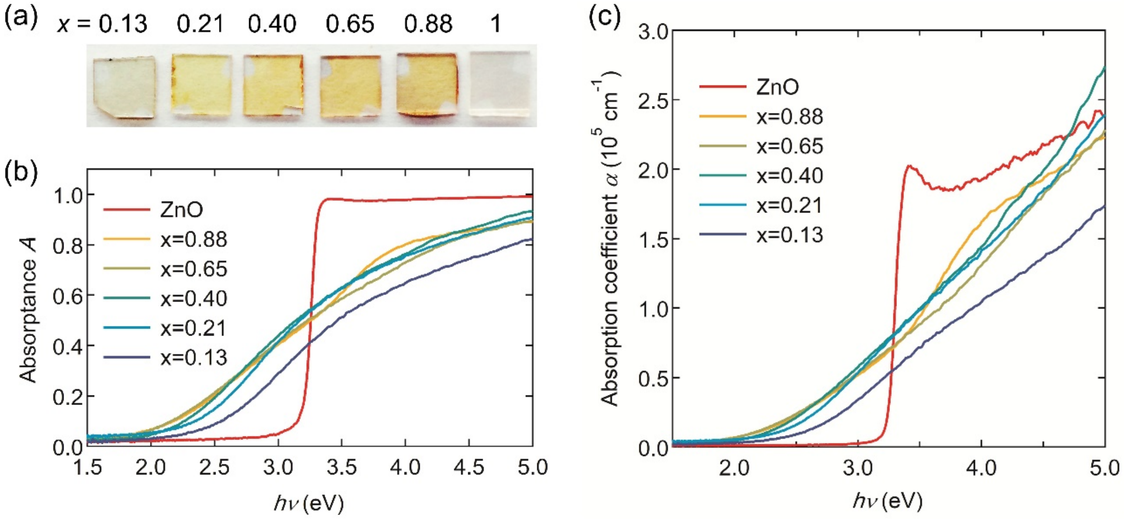

FIG. 4. (a) Photograph and (b) absorption spectra of $(GaN)_{1-x}(ZnO)_x$ thin films grown on Al_2O_3 substrates. (c) Absorption coefficients calculated from (b).

Previous DRS spectral shape analyses using Tauc plot suggested that $(GaN)_{1-x}(ZnO)_x$ is a direct-transition semiconductor.[10] However, absorption spectra here exhibited poor agreement with Tauc plots that assume a direct transition with the form $(\alpha h\nu)^2 \propto (h\nu - E_g)$ [Fig. 5]. A possible explanation for the discrepancy is that local structures, such as the short-range order of Zn-O/Ga-N pairs, are different because of the lower synthesis temperature.[31] Another reason may have been spectral shape distortion in the previous study due to the strong optical absorption of samples that were associated with data conversion from diffuse reflectance to absorbance by the Kubelka-Munk method.[32] High absorbance enhances the intensity of regular light reflection if it is not sufficiently diluted with a white standard. The reflection causes a difference in scattering factor between sample and standard, resulting in an underestimation of α. The latter was supported by the shape of the absorption spectrum of a diluted colloidal solution of $(GaN)_{0.27}(ZnO)_{0.73}$

nanocrystals: It was also inconsistent with a direct-transition semiconductor model (See Supplemental Material [24], Fig. S3), although the spectral shape has not been analyzed in the original report.[10]

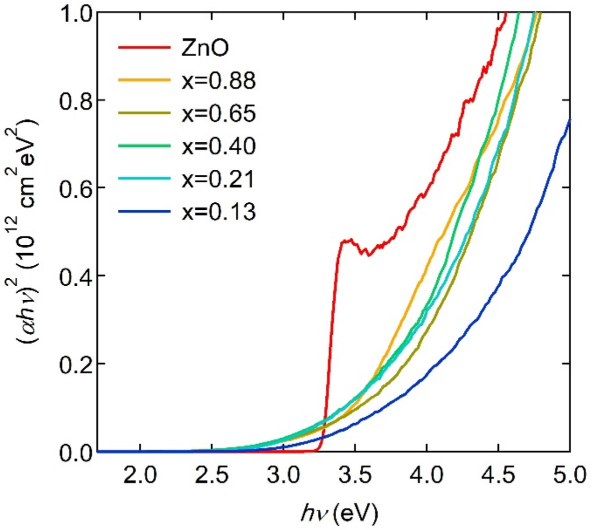

FIG. 5. Tauc plots of $(GaN)_{1-x}(ZnO)_x$ thin films grown on Al_2O_3 substrates, assuming a direct semiconductor model.

Despite the deviation in spectral shape, our thin films and the colloidal solution[25] exhibited 10^4-cm^{-1} α values, which were comparable to those for conventional direct transition semiconductors. It is known that Tauc plot analysis is invalid for the end members (GaN and ZnO) due to the strong contribution of exciton absorption. However, the solid solution ($0 < x < 1$) films showed broad and structureless absorption edges, indicating little contribution of exciton absorption. To investigate the origin of this inconsistency, we conducted first-principles calculations for $(GaN)_{1-x}(ZnO)_x$ (x=0, 0.25, 0.75, and 1). For each solid solution (x=0.25 or 0.75), three model structures of A, B, and C were prepared [Fig. 6(a) and Fig. 7(a)]: In model A, Zn (Ga) and O (N) form no Zn-O

(Ga-N) pair in the (2×2×1) supercell of GaN (ZnO). In model B, Zn (Ga) and O (N) form a Zn-O (Ga-N) pair in the (2×2×1) supercell of GaN (ZnO). In model C, Zn (Ga) and O (N) form a Zn-O-Zn-O (Ga-N-Ga-N) chain in the (2×2×2) supercell of GaN (ZnO). Fig. 6(b) shows the band dispersion diagrams of GaN and $(GaN)_{0.75}(ZnO)_{0.25}$. All three model structures of $(GaN)_{0.75}(ZnO)_{0.25}$ as well as GaN are direct-transition type semiconductors. However, the $(GaN)_{0.75}(ZnO)_{0.25}$ model structures showed rather flat valence-band top and narrower bandgap compared with GaN. The ZnO-rich $(GaN)_{0.25}(ZnO)_{0.75}$ model structures also showed flat valence-band top and narrower bandgap than ZnO [Fig. 7(b)]. We also calculated charge density maps of the valence band maximum at Γ point (see Fig. 6(b) and Fig. 7(b)), since the flat band suggests that localization of the orbital causes non-parabolicity in band structure. Fig. 6(c) and 7(c) indicated that the orbital of the valence band maximum was localized on N atoms bonded with Zn in both $(GaN)_{0.75}(ZnO)_{0.25}$ and $(GaN)_{0.25}(ZnO)_{0.75}$. These results suggest that formation of Zn-N bonds is an origin of the deviation of the spectral shape from the Tauc plot, because the Tauc plot analysis assumes parabolic shape for both conduction-band bottom and valence-band top.

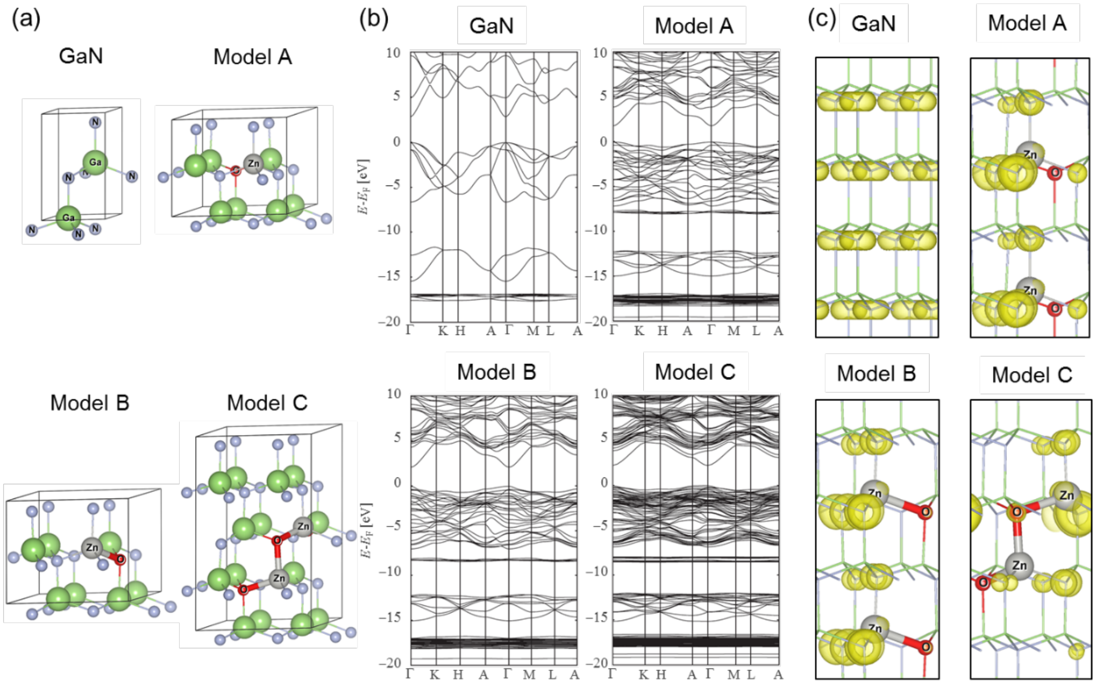

FIG. 6. (a) Optimized structures, (b) band dispersion diagrams, and (c) charge density maps of GaN and the three model structures of $(GaN)_{0.75}(ZnO)_{0.25}$. Green, blue, gray and red balls in (a) and (c) represent Ga, N, Zn and O atoms, respectively.

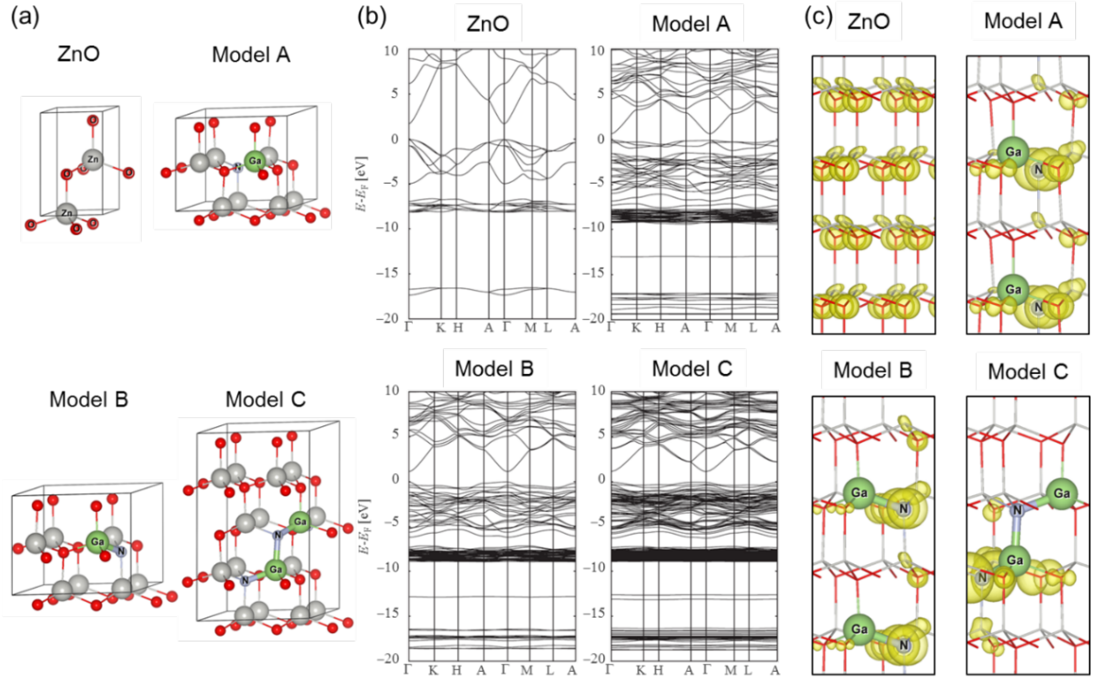

FIG. 7. (a) Optimized structures, (b) band dispersion diagrams, and (c) charge density maps of ZnO and the three model structures of $(GaN)_{0.25}(ZnO)_{0.75}$. Green, blue, gray and red balls in (a) and (c) represent Ga, N, Zn and O atoms, respectively.

Finally, we evaluated the compositional dependence of E_g of the $(GaN)_{1-x}(ZnO)_x$ thin films. Although the Tauc plot analysis does not have clear physical basis for systems with a localized valence band maximum as well as highly disordered structure similar to heavily isoelectronically doped compound semiconductors,[41] we practically used modified Tauc plots of $(\alpha h\nu)^{1/2} \propto (h\nu\text{-}E_g)$ for determining E_g because of their good linearity, as shown in Fig. 8(a). Fig. 8(b) revealed an asymmetric downward bowing of E_g, where E_g decreased with increasing x, with a minimum of ~2.0 eV at x=0.65. As mentioned above, the most GaN-rich film (x=0.13) was relatively over-oxidized. It is reported that excess oxygen in GaN forms a shallow donor level,[42] which might increase the E_g through bandgap renormalization and band filling effect as in the case of Si- or Ge-doped GaN.[43] However, in our most GaN-rich film, doped electrons were almost compensated probably due to formation of Ga vacancies and/or interstitial oxygens:[44,45] Its carrier concentration n_e, determined by Hall measurement, was 1.1×10^{19} cm^{-3}. Because the bandgap increase estimated from this n_e value was <60 meV,[43] we believe that the influence of the excess oxygen on E_g was relatively small.

Asymmetric band bowing similar to our results was recently reported for synthesized $(GaN)_{1-x}(ZnO)_x$ powders and nanocrystals having wide compositional ranges.[13,15,18] Although the asymmetric E_g dependence on x was not entirely understood,[8,19] it could be rationalized if the E_g reduction was more prominent in the ZnO-rich region relative to the GaN-rich region because of differences in the effective masses at the valence band maximum and the conduction band minimum.[8] Another speculation based on our theoretical calculation is that the reduction of E_g is caused by an increase of Zn-N bond. Table 1 summarizes the E_g obtained from the calculation. In both the GaN-rich and the ZnO-rich solid solutions, E_g decreases in the order of the model C, B, and A, where the number of Zn-N bonds increases in the same order. This tendency might suggest that formation of Zn-N bonds is kinetically more preferred in ZnO-rich composition than in GaN-rich one, although the absolute values of the E_g calculated in our study were inaccurate due to a well-known limitation of the LDA and exclusion of the contribution of excitonic absorption. Further analyses of E_g and α, combined with theoretical calculations for more accurate evaluation of E_g such as GW approximation with Bethe-Salpeter equation, is needed.

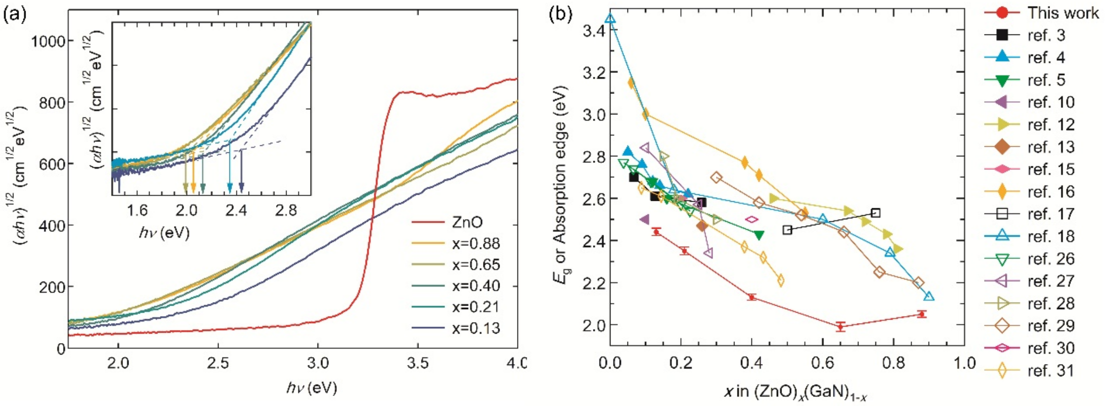

FIG. 8. (a) Tauc plots [$(\alpha h\nu)^{1/2}$ vs ($h\nu$-E_g)] of the $(GaN)_{1-x}(ZnO)_x$ solid solution thin films. Inset is the magnification around the absorption edges. (b) E_g of the $(GaN)_{1-x}(ZnO)_x$ solid solution thin films *vs. x*. Absorption edges reported in the literatures were also plotted for reference. Markers connected with solid lines are taken from the same report.

Table 1. E_g of the GaN, ZnO, and $(GaN)_{1-x}(ZnO)_x$ solid solutions (x=0.25 and 0.75) calculated from the band dispersion diagrams in Fig. 6(b) and 7(b).

Model	GaN	$(GaN)_{0.75}(ZnO)_{0.25}$			ZnO	$(GaN)_{0.25}(ZnO)_{0.75}$		
		A	B	C		A	B	C
Bandgap/ eV	2.90	1.81	2.13	2.25	1.77	0.75	1.14	1.18

IV. CONCLUSION

Epitaxial $(GaN)_{1-x}(ZnO)_x$ thin films were synthesized with multi-target PLD synchronized with a process gas supply control system. The single phase $(GaN)_{1-x}(ZnO)_x$ solid solution films were obtained by reducing the thickness of a GaN/ZnO pair in the GaN/ZnO superlattices to ~ 1 nm due to interlayer mixing. Low-temperature epitaxial growth enabled a wide-range compositional synthesis of the solid solution thin films. The solid solution thin films had large absorption coefficients ($>10^4$ cm^{-1}) in the visible light region. The shapes of the absorption edges were inconsistent with a direct bandgap. First-principles calculation suggested that this inconsistency originates from localization of the valence band maximum on N atoms bonded with Zn. The energy gap of the $(GaN)_{1-x}(ZnO)_x$ solid solutions empirically determined by modified Tauc plot exhibited asymmetric bowing with a ~2.0-eV minimum at x=0.65. These results demonstrated that low-temperature epitaxial growth was an effective synthesis of $(GaN)_{1-x}(ZnO)_x$ solid solutions with controlled chemical composition. This enabled a systematic study of fundamental physical properties. Although beyond the scope of this study, the fabricated GaN/ZnO superlattices could be useful for optoelectronic applications.

ACKNOWLEDGMENT

We thank Dr. Shoichiro Nakao for his assistance for optical measurements. This study was in part supported by CREST, Japan Science and Technology Agency (JST) (No. JPMJCR12C4) and the Grant-in-Aid for Scientific Research on Innovation Areas "Mixed anion" (JP16H06438, JP16H06441) from the Japan Society for the Promotion of Science (JSPS). C. Yang acknowledges the funding support from Deutsche Forschungsgemeinschaft Grant YA 511/1-1.

[1] A. J. Bard and M. A. Fox, Artificial photosynthesis: Solar splitting of water to hydrogen and oxygen, Accounts Chem. Res. **28**, 141 (1995).
[2] A. Fujishima and K. Honda, Electrochemical photolysis of water at a semiconductor electrode, Nature **238**, 37 (1972).
[3] K. Maeda, T. Takata, M. Hara, N. Saito, Y. Inoue, H. Kobayashi, and K. Domen, GaN:ZnO solid solution as a photocatalyst for visible-light-driven overall water splitting, J. Am. Chem. Soc. **127**, 8286 (2005).
[4] K. Maeda, K. Teramura, T. Takata, M. Hara, N. Saito, K. Toda, Y. Inoue, H. Kobayashi, and K. Domen, Overall water splitting on $(Ga_{1-x}Zn_x)(N_{1-x}O_x)$ solid solution photocatalyst: Relationship between physical properties and photocatalytic activity, J Phys Chem B **109**, 20504 (2005).
[5] K. Maeda, K. Teramura, D. L. Lu, T. Takata, N. Saito, Y. Inoue, and K. Domen, Photocatalyst releasing hydrogen from water, Nature **440**, 295 (2006).
[6] K. Maeda and K. Domen, New non-oxide photocatalysts designed for overall water splitting under visible light, J. Phys. Chem. C **111**, 7851 (2007).
[7] S. Z. Wang and L. W. Wang, Atomic and electronic structures of GaN/ZnO alloys, Phys. Rev. Lett. **104**, 065501 (2010).
[8] M. N. Huda, Y. F. Yan, S. H. Wei, and M. M. Al-Jassim, Electronic structure of ZnO:GaN compounds: Asymmetric bandgap engineering, Phys. Rev. B **78**, 195204 (2008).
[9] H. Pan and Y. W. Zhang, GaN/ZnO superlattice nanowires as photocatalyst for hydrogen generation: A first-principles study on electronic and magnetic properties, Nano Energ. **1**, 488 (2012).
[10] A. A. Reinert, C. Payne, L. M. Wang, J. Ciston, Y. M. Zhu, and P. G. Khalifah, Synthesis and characterization of visible light absorbing $(GaN)_{1-x}(ZnO)_x$ semiconductor nanorods, Inorg. Chem. **52**, 8389 (2013).
[11] K. Maeda and K. Domen, Solid solution of GaN and ZnO as a stable photocatalyst for overall water splitting under visible light, Chem. Mater. **22**, 612 (2010).
[12] S. C. Yan, Z. Q. Wang, Z. S. Li, and Z. G. Zou, Two-step reactive template route to a mesoporous ZnGaNO solid solution for improved photocatalytic performance, J. Mater. Chem. **21**, 5682 (2011).
[13] J. P. Wang, B. B. Huang, Z. Y. Wang, P. Wang, H. F. Cheng, Z. K. Zheng, X. Y. Qin, X. Y. Zhang, Y. Dai and M.-H. Whangbo, Facile synthesis of Zn-rich $(GaN)_{1-x}(ZnO)_x$ solid solutions using layered double hydroxides as precursors, J. Mater. Chem. **21**, 4562 (2011).

[14] M. Mapa, K. S. Thushara, B. Saha, P. Chakraborty, C. M. Janet, R. P. Viswanath, C. M. Nair, K. V. G. K. Murty, and C. S. Gopinath, Electronic structure and catalytic study of solid solution of GaN in ZnO, Chem. Mater. **21**, 2973 (2009).

[15] K. Lee, B. M. Tienes, M. B. Wilker, K. J. Schnitzenbaumer, and G. Dukovic, $(Ga_{1-x}Zn_x)(N_{1-x}O_x)$ nanocrystals: Visible absorbers with tunable composition and absorption spectra, Nano Lett. **12**, 3268 (2012).

[16] M. Zhong, Y. H. Ma, P. Oleynikov, K. Domen, and J. J. Delaunay, A conductive ZnO–ZnGaON nanowire-array-on-a-film photoanode for stable and efficient sunlight water splitting, Energ. Environ. Sci. **7**, 1693 (2014).

[17] M. Yang, Q. Huang, and X. Q. Jin, Microwave synthesis of porous ZnGaNO solid solution for improved visible light photocatalytic performance, Solid State Sci. **14**, 465 (2012).

[18] Y. G. Li, L. P. Zhu, Y. F. Yang, H. Song, Z. R. Lou, Y. M. Guo, and Z. Z. Ye, A full compositional range for a $(Ga_{1-x}Zn_x)(N_{1-x}O_x)$ nanostructure: High efficiency for overall water splitting and optical properties, Small **11**, 871 (2015).

[19] L. L. Jensen, J. T. Muckerman, and M. D. Newton, First-principles studies of the structural and electronic properties of the $(Ga_{1-x}Zn_x)(N_{1-x}O_x)$ solid solution photocatalyst, J. Phys. Chem. C **112**, 3439 (2008).

[20] W. Wei, Y. Dai, K. S. Yang, M. Guo, and B. B. Huang, Origin of the visible light absorption of GaN-rich Ga_{1-x} $Zn_xN_{1-x}O_x$ (x = 0.125) solid solution, J. Phys. Chem. C **112**, 15915 (2008).

[21] T. Hirai, K. Maeda, M. Yoshida, J. Kubota, S. Ikeda, M. Matsumura, and K. Domen, Origin of visible light absorption in GaN-rich $(Ga_{1-x}Zn_x)(N_{1-x}O_x)$ photocatalysts, J. Phys. Chem. C **111**, 18853 (2007).

[22] M. Yoshida, T. Hirai, K. Maeda, N. Saito, J. Kubota, H. Kobayashi, Y. Inoue, and K. Domen, Photoluminescence spectroscopic and computational investigation of the origin of the visible light response of $(Ga_{1-x}Zn_x)(N_{1-x}O_x)$ photocatalyst for overall water splitting, J. Phys. Chem. C **114**, 15510 (2010).

[23] E. J. McDermott, E. Z. Kurmaev, T. D. Boyko, L. D. Finkelstein, R. J. Green, K. Maeda, K. Domen, and A. Moewes, Structural and band gap investigation of GaN:ZnO heterojunction solid solution photocatalyst probed by soft X-ray spectroscopy, J. Phys. Chem. C **116**, 7694 (2012).

[24] See Supplemental Material at [URL will be inserted by publisher], which includes Refs. [3-5,10,12,13,15-18, 26-31]. Table S1 gives further details on the thicknesses of the GaN/ZnO pairs, the absorption edges of $(GaN)_{1-x}(ZnO)_x$ reported in the literatures are sumerized in FIG. S1, the absorption spectrum of $(GaN)_{1-x}(ZnO)_x$ thin films grown on ZnO substrates is shown in FIG. S2, and more information on the absorption spectrum and Tauc plots of a diluted colloidal solution of $(GaN)_{0.27}(ZnO)_{0.73}$ nanocrystals is provided in FIG. S3.

[25] C. H. Chuang, Y. G. Lu, K. Lee, J. Ciston, and G. Dukovic, Strong visible absorption and broad time scale excited-state relaxation in $(Ga_{1-x}Zn_x)(N_{1-x}O_x)$ nanocrystals, J. Am. Chem. Soc. **137**, 6452 (2015).

[26] X. Sun, K. Maeda, M. Le Faucheur, K. Teramura, and K. Domen, Preparation of $(Ga_{1-x}Zn_x)$ $(N_{1-x}O_x)$ solid-solution from $ZnGa_2O_4$ and ZnO as a photo-catalyst for overall water splitting under visible light, Appl. Catal. a-Gen. **327**, 114 (2007).

[27] H. Chen, W. Wen, Q. Wang, J. C. Hanson, J. T. Muckerman, E. Fujita, A. I. Frenkel, and J. A. Rodriguez, Preparation of $(Ga_{1-x}Zn_x)(N_{1-x}O_x)$ photocatalysts from the reaction of NH_3 with Ga_2O_3/ZnO and $ZnGa_2O_4$: In situ time-resolved XRD and XAFS studies, J. Phys. Chem. C **113**, 3650 (2009).

[28] H. Hashiguchi, K. Maeda, R. Abe, A. Ishikawa, J. Kubota, and K. Domen, Photoresponse of GaN:ZnO electrode on FTO under visible light irradiation, B. Chem. Soc. Jpn. **82**, 401 (2009).

[29] W. Q. Han, Z. X. Liu, and H. G. Yu, Synthesis and optical properties of GaN/ZnO solid solution nanocrystals, Appl. Phys. Lett. **96**, 183112 (2010).

[30] W. Q. Han, Y. Zhang, C. Y. Nam, C. T. Black, and E. E. Mendez, Growth and electronic properties of GaN/ZnO solid solution nanowires, Appl. Phys. Lett. **97**, 083108 (2010).

[31] H. Y. Chen, L. P. Wang, J. M. Bai, J. C. Hanson, J. B. Warren, J. T. Muckerman, E. Fujita, and J. A. Rodriguez, In situ XRD studies of ZnO/GaN mixtures at high pressure and high temperature: Synthesis of Zn-rich $(Ga_{1-x}Zn_x)(N_{1-x}O_x)$ photocatalysts, J. Phys. Chem. C **114**, 1809 (2010).

[32] G. Kortüm, W. Braun, and G. Herzog, Principles and techniques of diffuse-reflectance spectroscopy, Angew. Chem. Inter. Ed. Engl. **2**, 333 (1963).

[33] S. Shet, Y. F. Yan, N. Ravindra, J. Turner, and M. Al-Jassim, Photoelectrochemical behavior of mixed ZnO and GaN (ZnO:GaN) thin films prepared by sputtering technique, Appl. Surf. Sci. **270**, 718 (2013).

[34] S. Shet, Y. F. Yan, J. Turner, and M. Al-Jassim, Effect of gas ambient and varying RF sputtering power for bandgap narrowing of mixed (ZnO:GaN) thin films for solar driven hydrogen production, J. Power Sources **232**, 74 (2013).

[35] D. Drouin, A. R. Couture, D. Joly, X. Tastet, V. Aimez, and R. Gauvin, CASINO V2.42: a fast and easy-to-use modeling tool for scanning electron microscopy and microanalysis users, Scanning **29**, 92 (2007).

[36] G. Kresse and J. Furthmüller, Efficient iterative schemes for *ab initio* total-energy calculations using a plane-wave basis set, Phys. Rev. B, **54**, 11169 (1996).

[37] P. E. Blochl, Projector augmented-wave method, Phys. Rev. B **50**, 17953 (1994).

[38] J. P. Perdew and A. Zunger, Self-interaction correction to density-functional approximations for many-electron systems, Phys. Rev. B **23**, 5048 (1981).

[39] A. Kobayashi, H. Fujioka, J. Ohta, and M. Oshima, Room temperature layer by layer growth of GaN on atomically flat ZnO, Jpn. J. Appl. Phys. 2 **43**, L53 (2004).

[40] A. Sasaki, W. H. A. Matsuda, N. Tateda, S. Otaka, S. Akiba, K. Saito, T. Yodo, and M. Yoshimoto, Buffer-enhanced room-temperature growth and characterization of epitaxial ZnO thin films, Appl. Phys. Lett. 86, 231911 (2005).

[41] Y. Zhang, B. Fluegel, A. Mascarenhas, H. P. Xin, and C. W. Tu, Optical transitions in the isoelectronically doped semiconductor GaP:N: An evolution from isolated centers, pairs, and clusters to an impurity band, Phys. Rev. B 62, 4493 (2000).

[42] H. Wang and A.-B. Chen, Calculation of shallow donor levels in GaN, J. Appl. Phys. **87**, 7859 (2000).

[43] M. Feneberg, S. Osterburg, K. Lange, C. Lidig, B. Garke, R. Goldhahn, E. Richter, C. Netzel, M. D. Neumann, N. Esser, S. Fritze, H. Witte, J. Bläsing, A. Dadgar, and A. Krost, Band gap renormalization and Burstein-Moss effect in silicon- and germanium-doped wurtzite GaN up to 10^{20} cm^{-3}, Phys. Rev. B **90**, 075203 (2014).

[44] J. Oila, V. Ranki, J. Kivioja, K. Saarinen, P. Hautojärvi, J. Likonen, J. M. Baranowski, K. Pakula, T. Suski, M. Leszczynski, and I. Grzegory, Influence of dopants and substrate material on the formation of Ga vacancies in epitaxial GaN layers, Phys. Rev. B **63**, 045205 (2001).

[45] A. F. Wright, Substitutional and interstitial oxygen in wurtzite GaN, J. Appl. Phys. **98**, 103531 (2005).